# NUMERICAL SIMULATION OF AFP NIP POINT TEMPERATURE PREDICTION FOR COMPLEX GEOMETRIES

Kaishu Xia[1], Ramy Harik[1], Jeremy Herrera[1], Josh Patel[1] and Brian Grimsley[2]

[1] McNAIR Center for Aerospace Innovation and Research, Department of Mechanical Engineering, College of Engineering and Computing, University of South Carolina
1000 Catawba St., Columbia, SC, 29201, USA

[2] NASA Langley Research Center, Hampton, VA, 23681, USA

## ABSTRACT

Material placement at the ideal nip point temperature over complex surfaces with uniformity across the width of the compaction rollers results in optimized part properties for Automated Fiber Placement (AFP) processes. However, current AFP systems utilize heat control models and methodologies, based on multiple process parameters such as feed-rate and orientation, that are mostly open-loop. Here, infrared (IR) heater input is calibrated as a function of process parameters during machine qualification. This work presents a numerical simulation to predict arrayed-infrared (AIR) emitter radiation onto a substrate that includes view factor implementation, IR radiative heat flow calculation, energy rate balance, and a transient heat transfer model. The purpose of this numerical model is to predict nip point temperature on complex surfaces, serving as a baseline for a new arrayed-infrared (AIR) thermoset heater to improve AFP process control. It is anticipated that this simulation will accurately control the temperature for high-speed AFP layup of complex geometries. An anticipated result of an AIR heater system is that material calibration and testing will be reduced as temperature is instantaneously monitored and controlled. Therefore, temperature across the roller width will be uniform during placement of complex parts, independent of their geometry.

## 1. INTRODUCTION

Automated layup process technology is widely used as one of the aerospace composite manufacturing processes [1]. Automated Fiber Placement (AFP) is an example of an automated layup technology that is applied to complex geometries, as it lays narrow tows and can be steered over sharply curved surfaces, in the form of pucker and wrinkle defects, without buckling of fibers [2]. Before layup, the prepreg material needs to be pre-heated to sufficiently soften the uncured matrix, ensuring appropriate tackiness between the new layer and the substrate for secured layup. The process window is temperature dependent for thermoset materials [3]. Therefore, material layup at the ideal nip point temperature in a uniform fashion across the roller over the substrate surface facilitates maximizing structural properties.

There is ongoing research investigating infrared heater properties [4,5,6,7], production testing [8,9], in-situ surface inspection [10,11], and infrared (IR) heating control [12, 13, 14, 15]. The sensitivity of tack and dynamic stiffness of prepreg materials to both temperature and feed rate during the laminating process has been confirmed and demonstrated [8]. The use of an IR preheating technique on a thermoset prepreg Big Area Additive Manufacturing (BAAM) system was found to be an effective method for increasing the interlayer bond temperature and improving

the inter-laminar strength of printed components [16]. Calawa et al. [17], addressed the importance of highly controlled localized heating during high-speed thermoset AFP to prevent overheating due to an unexpected machine stop. It was noted that during AFP start-up and shut-down processes, the thermal effects also require investigation due to the increased power and short exposure time during high-speed AFP. Moreover, in high-speed AFP applications, there was concern that peak temperature was not accurately monitored due to the test machine capability.

Current AFP systems' heat control models and methodologies are mostly open-loop. For example, in the work of Stokes-Griffin et al. [18], an intensive trial-and-error approach was used in order to determine the most appropriate combination of process parameters for thermoplastic application. Di Francesco et al. [19] presented a validated semi-empirical model enabling open-loop control of the heater power as a function of the thermoplastic layup speed. Correlation between deposition temperature and process variables was obtained via a combination of experimental data and thermal modelling.

Meanwhile, research on closed-loop control for thermoplastic AFP is also in progress. Constrained model predictive control was utilized in Khan's work [20], in which future response of the thermal system was estimated by combining modelling prediction with real-time samples. At each sample, the future response was then optimized by manipulated variable adjustments. Therefore, accurate thermal prediction models with active control methodologies are needed to improve the efficiency and productivity of AFP technology.

This work outlines a solution to a radiative transient heat transfer problem during the AFP process. Since AFP deals with different complex geometries, particularly in aerospace applications, this proposed solution is expected to instantaneously predict nip point temperature across the width for complex tools. In addition, active radiation control and its effect on nip point temperature was demonstrated for the purpose of a uniform nip point temperature distribution independent of tool shape.

# 2. LITERATURE REVIEW

Heat input is one of the most sensitive variables affecting aerospace composite material fabrication [3]. Hence, a precise temperature prediction is imperative due to the limited AFP process window [3]. Radiative heating is used extensively in Automated Fiber Placement (AFP) technology as it is non-contact, has high heat flux affording fast response, is low cost, presents a safe operating environment, and utilizes simpler control methodology [21, 16, 22].

## 2.1 Industrial Infrared Heating

Infrared heating has grown in popularity throughout the aerospace industry as the preferred method of producing ideal material properties for AFP processes. It offers positive attributes such as better efficiency in open areas and less power consumption. Moreover, the energy savings and market factors where IR radiant heaters were used as a heating source have been investigated [21]. The patent by Gusakov [23] demonstrated a closed-loop controlled infrared heating system used in medical devices. The heating system [24] by Werdermann consisted of a preheating stage with an IR lamp to heat the tape's top side and one for the bottom side. Zaffro's automated tape laying heating system [25] has six bulbs along the incoming tape of three inches' width and another six along the thermoplastic tape. Churn [26] considered continuous curing of the deposited thermoset

material on the mandrel heated by an infrared bank. Yousefpour's thermoplastic composite C-Rings [27] were assisted by infrared material preheating. These examples of the extensive use of infrared heating systems underscores the importance of a precise infrared heating model.

## 2.2 Numerical Models

Sweeney et al. [28] proposed a transient thermal simulation including natural convection, radiation, and one-dimensional (1D) conduction to indicate how the process affects the thermoplastic composite IR heating. Recommendations were made on optimum process parameters for the purpose of reducing the heating cycle time for high speed thermoplastic material processing. Lee [29] studied heat transfer during thermoplastic composite tape lay-up process using a hot nitrogen-gas torch. Temperature distribution near the nip point region was measured and then simulated. It was found that a temperature deviation existed due to the oversimplified heat-transfer coefficient distribution near the nip point. Thus, a three-dimensional (3D) calculation including fluid flow analysis was suggested for more accurate prediction. Hassan et al. [30] developed a comprehensive simulation model of the two-step process during thermoset fiber placement composite manufacturing. The theoretic model utilized a 3D finite element thermal analysis correlated to an AFP process laying prepreg on a cylindrical mandrel. The measured temperature using embedded thermocouples agreed well with model predicted values. Chang et al. [31] developed a 3D transient infrared ray tracing thermal simulation that enabled the determination of the most efficient concentrative effect. Here, different configurations of infrared tungsten/halogen lamps and reflector geometries were compared, and the thermal properties of their combinations were measured during a mold surface heating process. Hörmann et al. [32] demonstrated the sensitive effect of the position and orientation of an IR emitter on the thermoset automated fiber process (TS-AFP) process. View factors and temperature distribution were approximated by discretization, and the proposed two-dimensional (2D) model was compared with experimental results. Lichtinger et al. [33] numerically simulated radiant effects during an experimental AFP process and correlated the influence of radiation distribution on adjacent tow-tape paths. Important approaches such as view factor calculation, transient implicit 1D finite difference (FD) and 3D finite element method (FEM) models were implemented. A multi-angle flat component layup thermal analysis was constructed and a 2D temperature gradient across the plate was found. Lichtinger [3] also provided an overview of AFP and its process parameters, and introduced an AFP offline programming procedure along with detailed research concerning AFP thermal management. This research work consists of a 3D FEM thermal flat surface model and dual experimental verification with both a thermal camera and a thermocouple. Finally, a thermal efficiency of 15.55% of heat input on the path of interest was estimated. A review [22] of development of radiative heating modeling in automated layup is presented. Compared to laser heating, less attention has been paid to infrared heating models. In most research work, the spatial dimension of heat transfer models has been reduced to simplify the computation work. Di Francesco et al. [19] reported a validated semi-empirical model where the associated experimental procedure and data reduction method determined the speed-dependent heater power function required to maintain the substrate surface temperature constant during variable speed layup. The model was based on simple measurements of the surface temperature during steady state layup for a range of heater powers and layup speeds. Correlation between deposition temperature and process variables were obtained via combination of experimental data and thermal modelling.

In this section, several research efforts on radiative heat transfer modelling are introduced and insights are provided. Lichtinger and Hörmann's models reduced heat transfer dimensions, by which the in-plane heat map cannot be constructed to illustrate a comprehensive nip point region. Here, in-plane heat conduction is considered as an important factor applied to complex surface geometries. Hörmann's published experimental setup and results also provide validation for proposed numerical model. Moreover, Chang's infrared ray tracing thermal simulation on different heater configurations serves as the baseline for proposed arrayed-infrared heating application. The accurate control of arrayed-infrared heating requires detailed studies on nip point region temperature change, thus the following section is devoted to the derivations of AFP heating numerical models.

# 3. NUMERICAL MODEL

The majority of research literature is not focused on AFP of complex geometries, which composes an essential part of aerospace structure manufacturing. The modeling of automated layup process heat transfer problems on complex surfaces requires the development of a thermal model with in-plane 2D heat flow. Moreover, radiation heat transfer involves interactions between two geometries with varying positions that must be calculated. Thus the concept of view factor [34] was introduced and numerically implemented in this paper. Here, view factor is defined as the radiative heat transfer proportion between two given geometries. Finally, to derive the correlation between the temperature distribution and both time and heater position, a numerical approach was required to solve the relevant partial differential equations.

## 3.1 Model Boundary Conditions

The boundary conditions are set similarly to Hörmann's experimental setup [32] shown in Figure 1. The Prepreg material and associated properties used in the simulations was Toray® T800S/3900-2. The AFP head operated at room temperature (20°C) with fixed IR lamps constantly heating the substrate (prepreg). The assembly of the IR heater was inclined at 20°degrees to the substrate material and a vertical distance of 78.7 mm to the roller nip point Here, conductions in 3D, both in-plane dimensions and thickness dimension, and convection on boundaries are considered. Forced convection was assumed to take place as the moving AFP head causes considerable air flow. The same heat transfer coefficients were assumed in reference to Hörmann's work. Radiation heat flux moves along the layup path with a velocity of 0.06 m/s. Heat transfer mechanisms and critical AFP dimensions are shown in Figure 1.

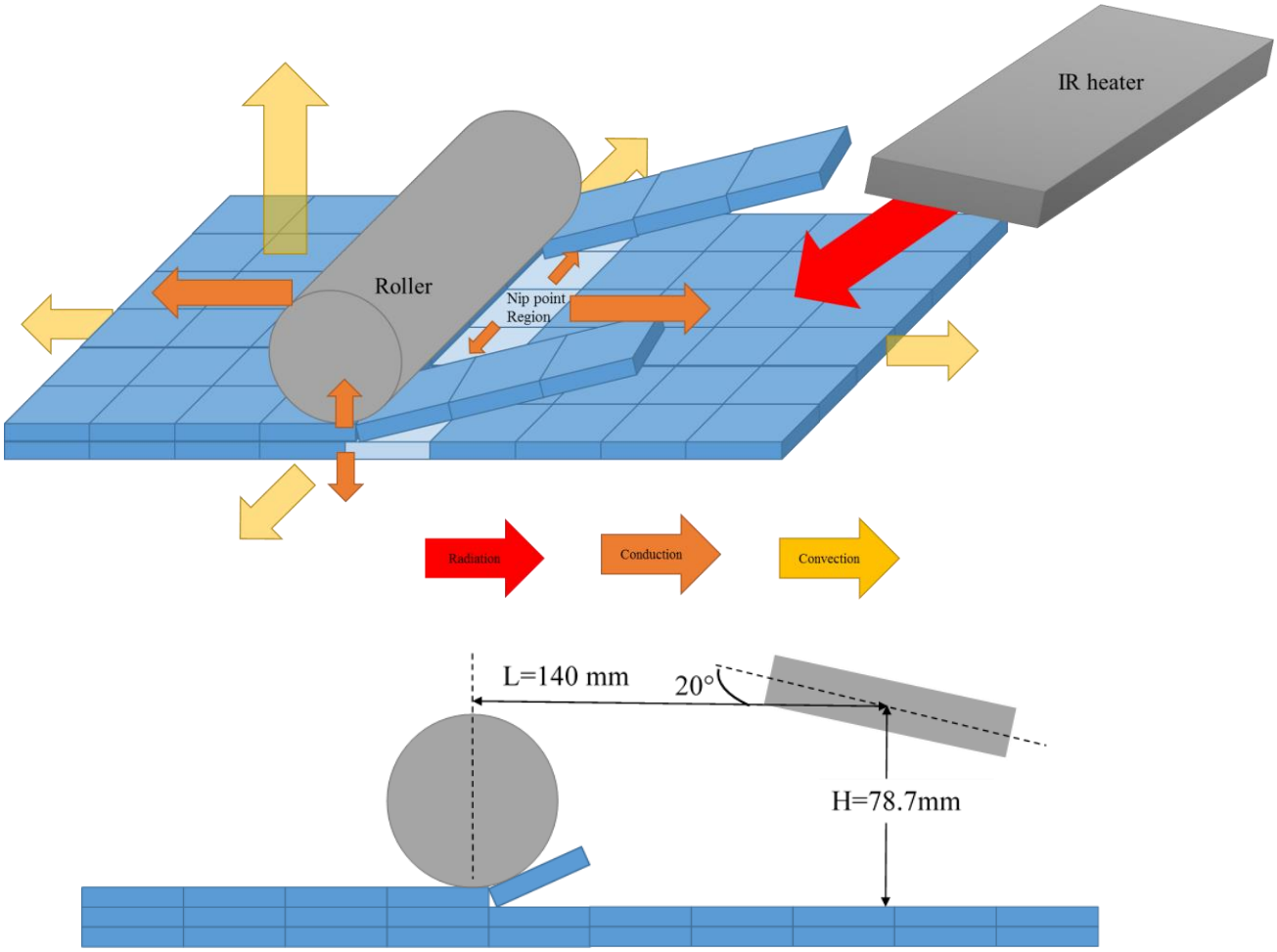


Figure 1. Heat transfer mechanisms (top) during automated layup process and critical dimensions in side view (bottom)

### 3.2 Derivation

Two important variables were estimated to derive substrate temperature distribution: view factors and IR radiative heat flow.

Based on literature [34], view factors were calculated using an integration method considering simple geometries and open surfaces, see Figure 2. View factors and temperature distribution are approximated by discretization.

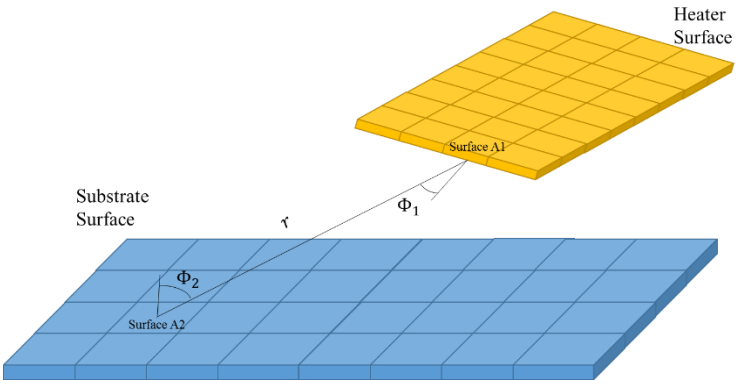


Figure 2. Integration Method in view factor implementation.

View factor $F_{12}$ represents fraction of energy leaving surface $A_1$ which reaches surface $A_2$. The equation [34] is represented as:

$$F_{12} = \frac{1}{\pi \cdot A_1} \int_{A_1} \int_{A_2} \frac{\cos(\Phi_1)\cos(\Phi_2)}{r^2} dA_2\, dA_1 \qquad [1]$$

Both the substrate and heater are discretized into mesh surfaces. In this case $\Phi_1$, $\Phi_2$ and $r$ are considered to be the same within each of the substrate mesh surfaces. By integrating all the view factors calculated with meshes on the substrate and heater surfaces, the view factor can be approximated as:

$$F_{12} = \frac{dA_2\, dA_1}{\pi \cdot A_1} \sum_m \sum_n \frac{\cos(\Phi_{1,\mathrm{mn}})\cos(\Phi_{2,\mathrm{mn}})}{\mathrm{r_{mn}}^2} \qquad [2]$$

The IR radiative heat flow calculated based on radiation heat transfer mechanism [32] is represented as:

$$q_{RA} = \frac{\sigma_B(T_{A1}^4 - T_{A2}^4)}{\frac{1-\varepsilon_1}{\varepsilon_1 \cdot A_1} + \frac{1}{F_{12} \cdot A_1} + \frac{1-\varepsilon_2}{\varepsilon_2 \cdot A_2}} = \frac{\eta \frac{q''_{IR,max}}{P_{EL,max}} P_{EL} - \sigma_B T_{A2}^4}{\frac{1-\varepsilon_1}{\varepsilon_1 \cdot A_1} + \frac{1}{F_{12} \cdot A_1} + \frac{1-\varepsilon_2}{\varepsilon_2 \cdot A_2}} \qquad [3]$$

Where:

$\varepsilon_1$: emissivity of surface $A_1$

$\varepsilon_2$: emissivity of surface $A_2$

$F_{12}$: view factor between surface $A_1$ and $A_2$

$q''_{IR,max}$: maximum heat flux provided by IR lamp manufacturer

$P_{EL,max}$: maximum electrical power

$P_{EL}$: electrical power input

$\sigma_B$: Stefan–Boltzmann constant

$\eta$: heater effectiveness

Temperature was derived by plugging equations [2] and [3] into the energy rate balance Equation [4] [32]. The approach to this transient heat transfer problem is by steady state approximation within very small time intervals.

$$q_{RA} - q_{CV} - q_{CD} = \rho \cdot V \cdot c_p \frac{dT}{dt} \quad [4]$$

Where:

$q_{RA}$: radiative heat flow

$q_{CV}$: convective heat flow

$q_{CD}$: conductive heat flow

$\rho$: substrate density

$V$: substrate element volume

$c_p$: substrate heat capacity

To solve Equation [3], a finite difference scheme (Figure 3) is used to discretize time as a variable, in which case the time step is considered as another dimension ($n$). An Implicit Method was utilized to derive for temperature at the next time step ($T_{i,j}^{n+1}$) by solving equation involving both temperature at current time step ($T_{i,j}^{n}$) and next time step ($T_{i+1,j}^{n+1}$, $T_{i-1,j}^{n+1}$, $T_{i,j+1}^{n+1}$, $T_{i,j-1}^{n+1}$). Heat transfer properties were set to be different in both directions, applicable to composite materials.

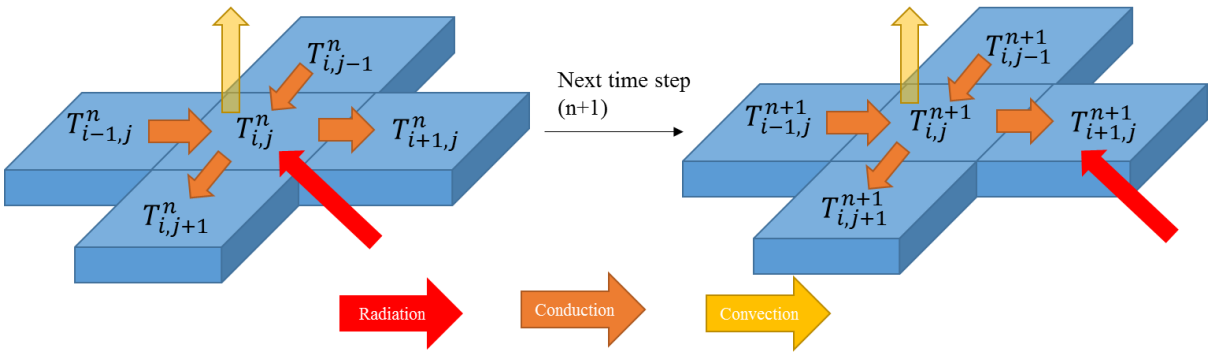

Figure 3. In-plane 2D heat flow solved by Finite Different Scheme.

Discretizing variables $i, j, n$, Equation [5]can be derived as:

$$\frac{A-\sigma_B\left(T_{i,j}^{n}\right)^4}{B+C+D}-\left(-E_x\left(T_{i+1,j}^{n+1}-2T_{i,j}^{n+1}+T_{i-1,j}^{n+1}\right)-E_y\left(T_{i,j+1}^{n+1}-2T_{i,j}^{n+1}+T_{i,j-1}^{n+1}\right)\right) - F\left(T_{i,j}^{n}-T_{EN}\right)=G\left(T_i^{n+1}-T_i^{n}\right) \quad [5]$$

Where:

$$A=\eta_H\frac{q_{IR,max}^{"}}{P_{EL,max}}P_{EL},\ B=\frac{1-\varepsilon_1}{\varepsilon_1\cdot A_1},C=\frac{1-\varepsilon_2}{\varepsilon_2\cdot A_2},\ D=\frac{1}{F_{12}\cdot A_1},\ F=h_{cv}A_{CV},\ G=\frac{\rho\cdot V\cdot c_p}{dt},$$

$$E_x=\frac{k_x}{\Delta x^2}A_{cd\_x}\ ,\ E_y=\frac{k_y}{\Delta y^2}A_{cd\_y}$$

Rearranging Equation [5]:

$$\frac{A}{B+C+D}+FT_{EN}+(G-F)T_{i,j}^{n}-\frac{\sigma_B}{B+C+D}\left(T_{i,j}^{n}\right)^4 = -E_x\left(T_{i+1,j}^{n+1}+T_{i-1,j}^{n+1}\right)-E_x\left(T_{i,j+1}^{n+1}+T_{i,j-1}^{n+1}\right)+(2E_x+2E_y+G)T_{i,j}^{n+1}$$

In matrix form:

$$\left[T_{i,j}^{n+1}\right]=\ [A_{CV,CD,S}]^{-1}[[b]+[A_S]\left[T_{i,j}^{n}\right]-[A_{RA}][(T_{i,j}^{n})^4]] \quad [6]$$

# 4. RESULTS

In this section, models were simulated for both flat and complex surfaces. The following examples and their validation were provided to demonstrate the potential application of proposed thermal modeling of variable geometries. To ensure accurate model validation, simulations were compared with published experimental research work. Thermal modeling and numerical simulations allowed for accurate predictions of necessary view factor calculations and resulting nip point temperatures.

## 4.1 AFP on Flat Surface

A numerical simulation of Equation [6] was implemented in *MATLAB*® software. This solution was tested both on flat surfaces in Figures 4-8 and complex geometry in Figures 9-12. Figures 4 and 5 represent the computation of the view factors and temperature, based on our numerical implementation. Figure 4 describes view factors distribution at 5$^{th}$ time step (top) and 50$^{th}$ time step (bottom). A heat map at nip point region at 50$^{th}$ time step is shown in Figure 5. Figure 6 provides a validation of the model. By comparing Hörmann's experimental results [32] with the proposed simulation, with the same experimental configuration, the proposed thermal simulation results accurately predict a maximum nip point temperature change ($\Delta T$=27.49 °C). However, the temperature change duration was considerably shorter than the experimental results due to the above steady state approximation to Eq. [4]. This approximation approach has neglected thermal

system response caused by heat transfer lag and a deviation in time scale exists herein. For example, with regard to temperature history in Figure 6, within one time interval (0.1 sec), this steady state model simulates a temperature rise up to 7 °C, which may take heated substrate more than 0.1 second to rise up to that temperature. In order to improve the model accuracy, a thermal system response time depending on heated object dimension and properties needs to be considered as one of the important factors in high speed layup processes.

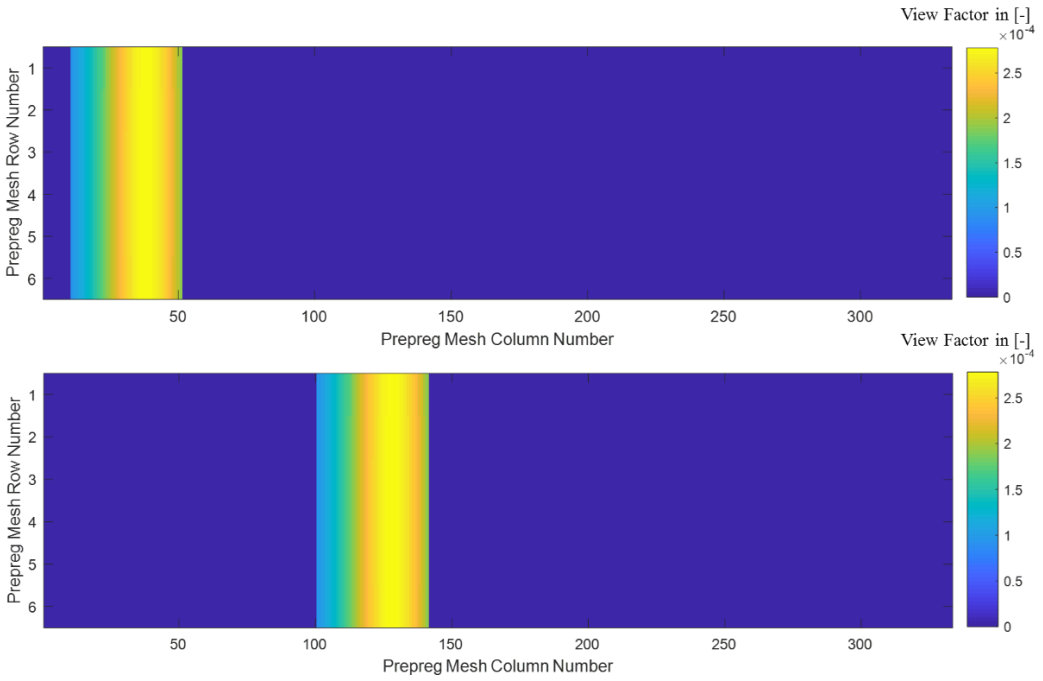


Figure 4. View Factors distribution at time step=5 (top) and at time step=50 (bottom) on flat surface.

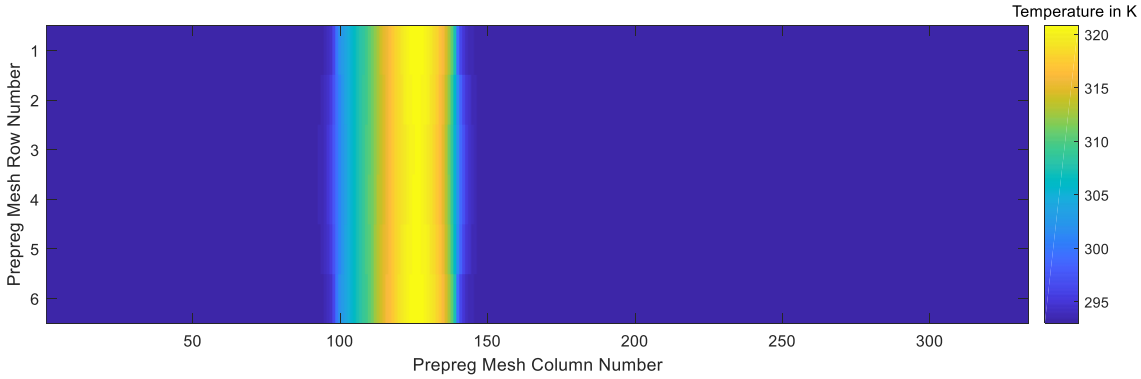


Figure 5. In-plane 2 dimensional temperature distribution (unit: K) at time step=50 on flat surface.

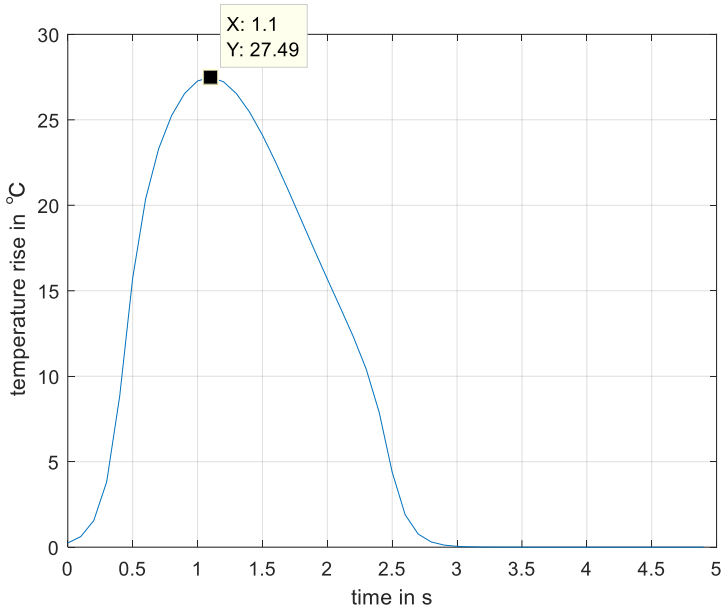


Figure 6. Temperature change comparison on one fixed point simulated by proposed model (ΔT=27.49 °C) with Hörmann's experimental results [32] (ΔT~=24 °C).

The proposed model also predicts the effect of infrared radiation control on nip point temperature (Figures 7-8). An Arrayed-Infrared (AIR) heater configuration can be utilized as the heat source during the AFP process, where each component IR heater can be controlled individually in response to the signal from process parameter sensors such as an IR camera. Power was calculated by the proposed prediction model and then exerted on the AIR heaters, permitting precise and immediate process control.

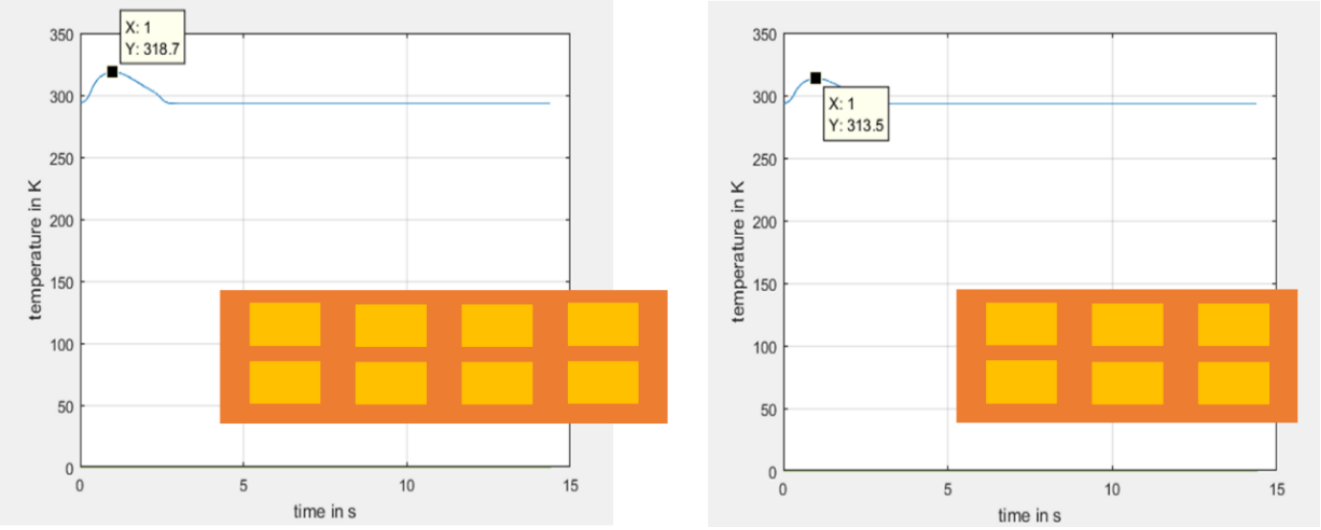


Figure 7. Comparing temperature change on a single fixed point simulated by two different AIR heater configurations (Left: 4 by 2; Right: 3 by 2).

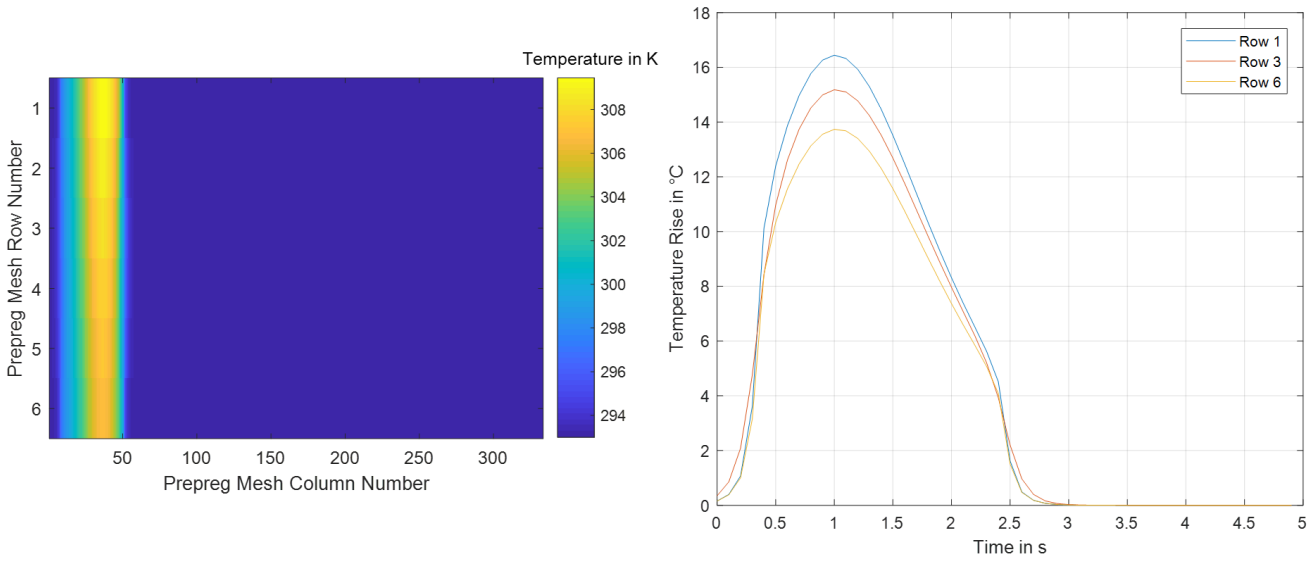


Figure 8. Temperature distribution on three observation points with Controlled AIR heaters (AIR Configuration: 4 by 2, in which 4 emitters ON and others OFF).

## 4.2 AFP on Complex Geometry

The geometry shown in Figure 9 was used to designate layup geometry and path. The same numerical model simulated the processing of the given layup designs in Figure 9, and the in-plane temperature distribution was obtained. The Eulerian model was implemented to locate heater position, given nip point position on the path as shown in Figure 10.

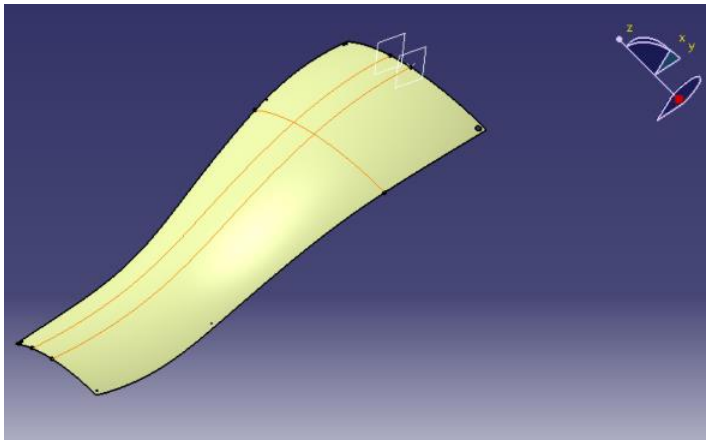

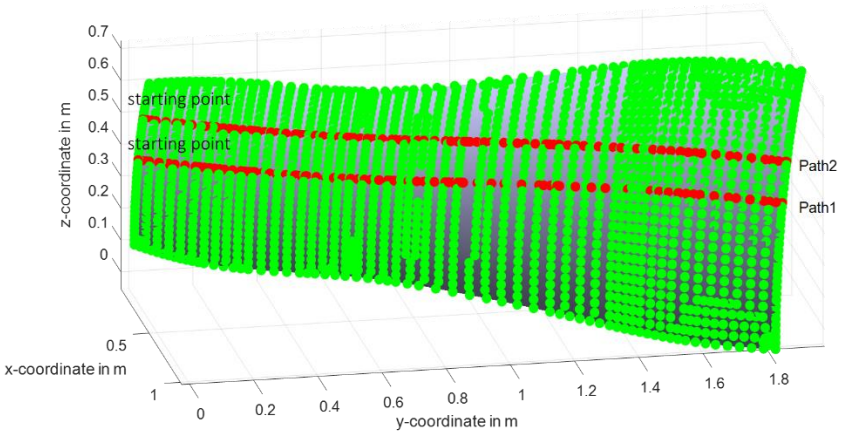


Figure 9. CAD model of complex geometry and designed paths (Left) and import surface and path1 data to MATLAB from CAD (Right).

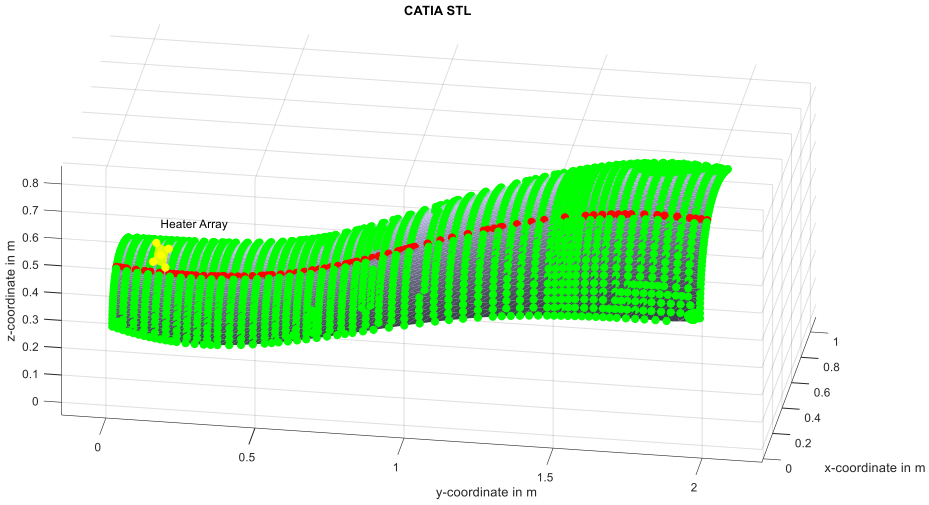


Figure 10. Locating AIR heaters by nip points on Path 1.

Layups along Path 1 and Path 2 are simulated with the proposed model. As in Figure 9, Path 1 is on geometric mid-plane while path 2 is generated by a certain offset value from Path 1. Therefore, Path 2 possesses more geometric asymmetry, which was verified by the view factors distribution map demonstrated in Figure 11. With the same process configuration as the flat surface case, in-plane temperature distribution with time steps along Path 1 was computed and shown in Figure 12**.** The temperature distribution simulated on complex surface demonstrates significant temperature variations along both directions. The temperature distribution agrees well with geometry as in Figure 12. By looking at substrate geometry and designated paths in Figure 9, one can find that radiation distributes symmetrically along Path 1. While on Path 2, asymmetry of radiation on path at starting point was strong and reduced gradually in first 10 steps. This radiation trend can also be found in view factor (Figure 11) and temperature (Figure 12) distribution simulated with this model.

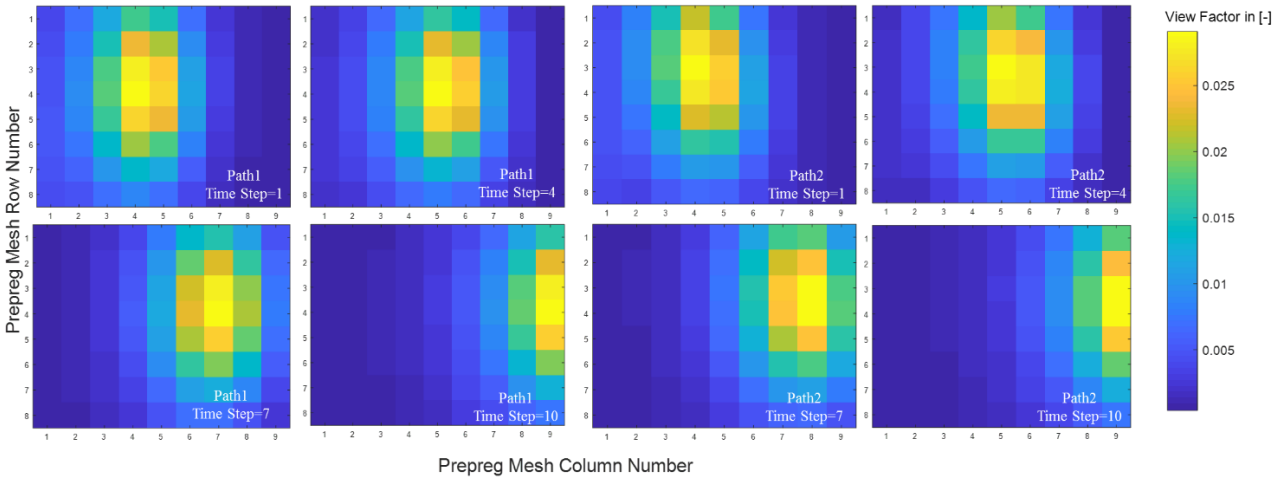


Figure 11. Path1 (left) and Path2 (right) view factors distribution at time step 1, 4, 7, 10

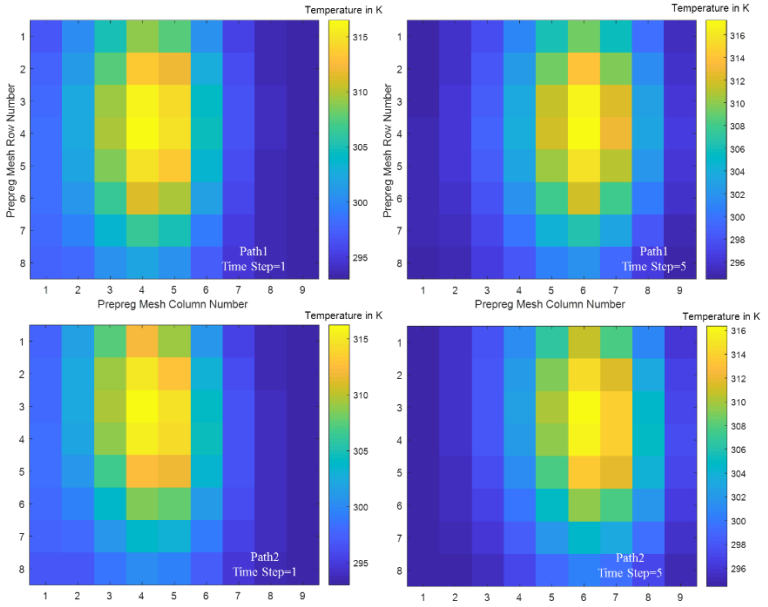


Figure 12. Temperature distribution at time step 1, 5 on Path 1 and Path 2

## 5. CONCLUSIONS

A solution to the AFP transient radiative heat transfer problem was proposed in this work. A literature review was conducted to adapt and improve upon established methods of solving this problem. Finding and predicting process variables such as view factor and IR radiative heat flow, leaded to the development of thermal modeling implemented in this work. This modeling allows for accurate nip point temperature predictions for simple and complex tooling. A numerical solution to address 2D in-plane heat transfer problems was derived. Simulation results were obtained in form of both in-plane temperature and temperature history and compared with published experimental results [32]. A maximum nip point region temperature change of 27.49 °C

was predicted with standard configuration in [32]. Moreover, this work provides the path to potential control methodology for AFP heating, particularly applicable to real-time monitoring and controlling nip point temperature distribution on complex tool surfaces.

Future work on this topic includes the thermal response time that has not been considered by steady state approximation. Shadow effects on complex surfaces will also need to be addressed and solved. Meanwhile, complex interaction between process parameters also requires further study to acquire better understanding of their effects in high speed layup processes. The results found will be utilized for understanding the effect of different AIR configurations and positioning of the heat source in relation to the substrate surface being heated. Finally, control methodologies for AIR heating devices can be developed and improved to enable higher product quality with lower power consumption. To obtain temperature uniformity, the power control of the heat source was optimized attending to IR heater response time. By testing different AIR configurations, the controllability of each individual IR heater power input, $P_{EL}$, will be essential for a uniform nip point temperature distribution throughout complex geometries.

## 6. ACKNOWLEDGMENTS

The authors thank Benjamin Greenberg, undergraduate research assistant and McNAIR Junior Fellow at the University of South Carolina, for his research support. The authors express their utmost gratitude to NASA and Advanced Composites Project for supporting this research.

## 7. REFERENCES

1. NASA: "Design and Manufacturing Guideline for Aerospace Composites." *l. NASA*, 2005.
2. Wilson, C., & Mcgranaghan, G. "Infrared heating comes of age." *Reinforced Plastics* 58(2) (2014): 43-47.
3. Lichitinger, Roland. "Thermal Simulation of Automated Fiber Placement Process and its Validation." *Symposium on the occasion of the 5th anniversary of the Institute for Carbon Composites*, Munich, 2014.
4. Masanori, Konishi, "Infrared light bulb, heating device, production method for infrared light bulb", U.S. Patent 6654549 B1, Nov. 25, 2003.
5. Denkena, B., Schmidt, C., Völtzer, K., & Hocke, T. "Thermographic online monitoring system for Automated Fiber Placement processes." *Composites Part B: Engineering* 97 (2016): 239-243.
6. Witek, K., Piotrowski, T., & Skwarek, A. "Analysis of polymer foil heaters as infrared radiation sources." *Materials Science and Engineering: B* 177(15) (2012): 1373-1377.
7. Hsieh, C., Tzou, D., Huang, Z., Hsu, J., & Lee, C. "Decoration of zinc oxide nanoparticles onto carbon fibers as composite filaments for infrared heaters." *Surfaces and Interfaces* 6 (2017): 98-102.
8. Crossley, R., Schubel, P., & Focatiis, D. D. "Time–temperature equivalence in the tack and dynamic stiffness of polymer prepreg and its application to automated composites manufacturing." *Composites Part A: Applied Science and Manufacturing* 52 (2013): 126-133.
9. Endruweit, A., De Focatiis, D. S. A., Ghose, S., Johnson, B. A., Younkin, D. R. and Warrior, N. A. "In Characterization of Prepreg Tack to Aid Automated Material Placement." *SAMPE Technical Meeting*, Long Beach, CA United States of America, May 23-26, 2016.

10. Juarez, P. D., Cramer, K. E., & Seebo, J. P. “Advances in in situ inspection of automated fiber placement systems.” *Thermosense: Thermal Infrared Applications XXXVIII* (2016).
11. Oromiehie, E., Prusty, B. G., Compston, P., & Rajan, G. “In-situ simultaneous measurement of strain and temperature in automated fiber placement (AFP) using optical fiber Bragg grating (FBG) sensors.” *Advanced Manufacturing: Polymer & Composites Science* 3(2) (2017): 52-61.
12. Adonis, M., Khan, MTE. “PID control of infrared radiative power profile for ceramic emitters”, *2003 IFAC.*
13. Shekher, V., Rai, P., Prakash, O. “Design and Evaluation of Classic PID, Gain and Phase Margin Based Controller and Intelligent Controller Design for a Ceramic Infrared Heater.” *ARPN Journal of Science and Technology* 3(2) (2012): 248-256.
14. Martínez, S., Lamikiz, A., Ukar, E., Tabernero, I., & Arrizubieta, I. “Control loop tuning by thermal simulation applied to the laser transformation hardening with scanning optics process.” *Applied Thermal Engineering* 98 (2016): 49-60.
15. Wilson, J., Everett, S., Dubay, R., Parsa, S. S., & Tyler, M. “Spatial predictive control using a thermal camera as feedback.” *Measurement* 109 (2017): 384-393.
16. Kishore, V., Ajinjeru, C., Nycz, A., Post, B., Lindahl, J., Kunc, V., & Duty, C. “Infrared preheating to improve interlayer strength of big area additive manufacturing (BAAM) components.” *Additive Manufacturing* 14 (2017): 7-12.
17. Calawa, R., & Nancarrow, J. “Medium Wave Infrared Heater for High-Speed Fiber Placement.” *SAE Aerofast* (2007). Los Angeles, CA, USA.
18. Stokes-Griffin, C., & Compston, P. “The effect of processing temperature and placement rate on the short beam strength of carbon fibre–PEEK manufactured using a laser tape placement process.” *Composites Part A: Applied Science and Manufacturing* 78 (2015): 274-283.
19. Francesco, M. D., Veldenz, L., Dellanno, G., & Potter, K. “Heater power control for multi-material, variable speed Automated Fibre Placement.” *Composites Part A: Applied Science and Manufacturing* 101 (2017): 408-421.
20. Khan, Salman. (2011). “Thermal control system design for automated fiber placement process.” Doctoral Dissertation, *Concordia University*, Montreal, QC, Canada.
21. Dudkiewicz, E., & Jeżowiecki, J. “Measured radiant thermal fields in industrial spaces served by high intensity infrared heater.” *Energy and Buildings* 41(1) (2009): 27-35.
22. Orth, T., Weimer, C., Krahl, M., & Modler, N. “A review of radiative heating in automated layup and its modelling.” *Journal of Plastics Technology* 2(2017): 91-125.
23. Gusakov, I. “Infrared heating system for surgical patients.” Patent, 4969459, Published: Nov 13, 1990.
24. Werdermann, C., Friedrich, K., Cirino, M. & Pipes, B. “Design and Fabrication of an On-Line Consolidation Facility for Thermoplastic Composites.” *Journal of Thermoplastic Composite Materials* 2 (1989): 293-306.
25. Zaffiro, P. A. “Control of Radiant Heating System for Thermoplastic Composite Tape.” Patent, US005177340A, Published: January 5, 1993.
26. Chern, B., Moon, T. & J. Howell, J. R. “Thermal Analysis of In-Situ Curing for Thermoset Hoop-Wound Structures Using Infrared Heating: Part I – Predictions Assuming Independent Scattering.” *Journal of Heat Transfer* 117(3) (1995): 674.
27. Yousefpour, A., Ghasemi Nejhad, M. N. “Experimental and Computational Study of APC-2/AS2 Thermoplastic Composite C-Rings.” *Journal of Thermoplastic Composite Materials* 14 (2) (2001): 129-145.

28. Sweeney, G., Monaghan, P., Brogan, M. & Cassidy, S. “Reduction of infra-red heating cycle time in processing of thermoplastic composites using computer modelling.” *Composites Manufacturing* 6(3-4) (1995): 255-262.
29. Lee, M. “Heat transfer and consolidation modeling of composite fiber tow in fiber placement,” Ph.D. dissertation, *Virginia Polytechnic Institute & State University*, Virginia, 2004.
30. Hassan, N., Thompson, J.E. & Batra, R.C. “A heat transfer analysis of the fiber placement composite manufacturing process.” *J. Reinf. Plastics Compos* 24 (2005): 869-888.
31. Chang, P., Hwang, S. “Simulation of infrared rapid surface heating for injection molding.” *International Journal of Heat and Mass Transfer* 49(21-22) (2006): 3846-3854.
32. Hörmann, P., Stelzl, D., Lichtinger, R., Van Nieuwenhove, S., Mazón Carro, G. & Drechsler, K. “On the numerical prediction of radiative heat transfer for thermoset automated fiber placement.” *Composites: Part A* 67 (2014): 282–288.
33. Lichtinger, R., Hörmann, P., Stelzl, D., & Hinterhölzl, R. “The effects of heat input on adjacent paths during Automated Fibre Placement.” *Composites Part A: Applied Science and Manufacturing* 68 (2015): 387-397.
34. Gupta, M. K., Bumtariya, K. J., Shukla, H., Patel, P., & Khan, Z. “Methods for Evaluation of Radiation View Factor: A Review.” *Materials Today: Proceedings*, 4(2) (2017): 1236-1243.